ExoMol line lists – XLVI: Empirical rovibronic spectra of silicon mononitrate (SiN) covering the 6 lowest electronic states and 4 isotopologues

Mikhail Semenov[1], Nicholas Clark[1], Sergei N. Yurchenko[1], Gap-Sue Kim[2], Jonathan Tennyson[1]*

[1] *Department of Physics and Astronomy, University College London, Gower Street, WC1E 6BT London, UK*
[2] *Dharma College, Dongguk University, 30, Pildong-ro 1-gil, Jung-gu, Seoul 04620, Korea*

13 July 2022

ABSTRACT

Silicon mononitride (^{28}Si^{14}N, ^{29}Si^{14}N, ^{30}Si^{14}N, ^{28}Si^{15}N) line lists covering infrared, visible and ultraviolet regions are presented. The SiNful line lists produced by ExoMol include rovibronic transitions between six electronic states: $X\,^2\Sigma^+$, $A\,^2\Pi$, $B\,^2\Sigma^+$, $D\,^2\Delta$, $a\,^4\Sigma^+$, $b\,^4\Pi$. The *ab initio* potential energy and coupling curves, computed at the multireference configuration interaction (MRCI/aug-cc-pVQZ) level of theory, are refined for the observed states by fitting their analytical representations to 1052 experimentally derived SiN energy levels determined from rovibronic bands belonging to the X–X, A–X and B–X electronic systems through the MARVEL procedure. The SiNful line lists are compared to previously observed spectra, recorded and calculated lifetimes, and previously calculated partition functions. SiNful is available via the www.exomol.com database.

Key words: molecular data, opacity, astronomical data bases: miscellaneous, planets and satellites: atmospheres, stars: low-mass.

1 INTRODUCTION

Silicon is considered to be the second most abundant element in Earths crust (CRC Handbook 2016) and the seventh most abundant element on the planet according to McDonough & Sun (1995); low silicon abundance within a host is considered to be a better indicator of a potential planet detection than planet-metallicity correlation according to Brugamyer et al. (2011). So far there have been multiple observations of SiN in different media in space: interstellar medium (Schilke et al. 2003; Turner & Dalgarno 1977; Feldman et al. 1983), red giant stars (Davis 1947; Gratton 1952), and envelopes of carbon stars (Turner 1992). Apart from being an important astrophysical species, SiN has multiple different applications: quantum dot production (Xie et al. 2017), quantum optomechanics (Serra et al. 2018), protective coating for biological tissues and dental implants (Pettersson et al. 2013; Raza et al. 2020), membranes used in filtering and biosensor systems (Vlassiouk et al. 2009; Lee et al. 2014).

The SiN molecule seems to be well studied experimentally in comparison to some of its valence group counterparts. Originally the molecule was reported by Jevons (1913), with band heads attributed to the $B\,^2\Sigma^+$–$X\,^2\Sigma^+$ band. Later Mulliken (1925) conducted a more thorough study of the $B\,^2\Sigma^+$–$X\,^2\Sigma^+$ reporting rotational transitions and detecting a weaker band later identified as $C\,^2\Pi$–$X\,^2\Sigma^+$ thanks to additional experimental works conducted by Linton (1975). Overall the main active electronic bands that have been rotationally resolved so far are $B\,^2\Sigma^+$–$X\,^2\Sigma^+$ (Ojha & Gopal 2013; Ito et al. 1993; Naulin et al. 1993; Piper & Caledonia 1991; Foster 1989; Walkup et al. 1984; Foster 1984; Bredohl et al. 1976; Singh et al. 1973; Dunn et al. 1969; Nagaraj & Verma 1968; Schofield & Broida 1965; Stevens & Ferguson 1963; Jenkins & de Laszlo 1928),

---

* The corresponding author: j.tennyson@ucl.ac.uk

$A\,^2\Pi$–$X\,^2\Sigma^+$ (Meloni et al. 2004; Elhanine et al. 1992; Foster 1989; Yamada et al. 1988; Yamada & Hirota 1985; Foster et al. 1985; Foster 1984; Bredohl et al. 1976; Jevons 1913) and $C\,^2\Pi$–$X\,^2\Sigma^+$ (Foster 1989; Bredohl et al. 1976; Linton 1975; Mulliken 1925), $B\,^2\Sigma^+$–$A\,^2\Pi$ (Bredohl et al. 1976). Of these Ojha & Gopal (2013) is the most recent experimental study, which apart from the $B\,^2\Sigma^+$–$X\,^2\Sigma^+$ band mentioned earlier, has also been able to detect and vibrationally resolve the $f\,^4\Sigma^-$–$d\,^4\Sigma^-$, $b\,^4\Pi$–$d\,^4\Sigma^-$. Additionally we want to highlight that Nagaraj & Verma (1968) originally assigned their spectrum and quantum numbers to the SiO$^+$ anion, however, that was later corrected by the Dunn et al. (1969) and assigned to the $B\,^2\Sigma^+$–$X\,^2\Sigma^+$ band of SiN.

A large number of theoretical investigations of SiN have been performed since the discovery of the molecule (Xing et al. 2018, 2013; Oyedepo et al. 2011; Li et al. 2009; Kerkines & Mavridis 2005; Jungnickel et al. 2000; Singh et al. 1999; Cai et al. 1998; Borin 1996; Chong 1994; Chen et al. 1993; Mclean et al. 1992; Curtiss et al. 1991; Melius & Ho 1991; Muller-Plathe & Laaksonen 1989; Ziurys et al. 1984; Bruna et al. 1984; Preuss et al. 1978; Gohel & Shah 1975). The most recent *ab initio* work at the time of writing was carried out by Xing et al. (2018) who conducted a thorough analysis of the transition dipole moment curves and potential energy curves for the lowest 8 doublets ($X\,^2\Sigma^+$, $A\,^2\Pi$, $B\,^2\Sigma^+$, $C\,^2\Pi$, $D\,^2\Delta$, $E\,^2\Delta$,$F\,^2\Pi$, $G\,^2\Delta$), of SiN, additionally reporting on Frank-Condon factors and lifetimes for the first 15 vibrational levels of each electronic state, for which they used program LEVEL due to Le Roy (1998). The states were studied at the Internally Contracted Multirefrence Configuration Interaction with Davidson correction (icMRCI+Q) level with additional extrapolation procedure employed as described by Oyeyemi et al. (2014). A lot of work in the 2018 paper was built on the foundation of their earlier paper (Xing et al. 2013), where they reported PECs for the lowest 8 doublets ($X\,^2\Sigma^+$, $A\,^2\Pi$, $B\,^2\Sigma^+$, $C\,^2\Pi$, $D\,^2\Delta$, $E\,^2\Delta$, $F\,^2\Pi$, $G\,^2\Delta$) and 4 quartets ($a\,^4\Sigma^+$, $b\,^4\Pi$, $c\,^4\Delta$, $d\,^4\Sigma^-$) and the lowest sextet state $1\,^6\Sigma^+$. Apart form PECs this paper also reported spectroscopic constants and discussed the effects of the spin-orbit couplings.

The work described below will present original *ab initio* potential energy curves (PECs), spin-orbit curves (SOCs), electronic angular momentum curves (EAMCs) and (transition) dipole moment curves (DMCs) calculated using a high level of theory with MOLPRO (Werner et al. 2020) and then empirically fitted using data obtained from a MARVEL (measured active rotation vibration energy levels) (Furtenbacher et al. 2007) procedure and generated from effective Hamiltonians using PGOPHER (Western 2017). The refined spectroscopic model is then used to compute molecular line lists for four isotopologues of SiN. Both the refinement and line list calculations are performed using the rovibronic program Duo (Yurchenko et al. 2016). We then use our line lists to give high accuracy comparison to previously reported experimental spectra, calculated and experimental lifetimes, and partition function.

2   *Ab initio* MODEL

In this work six lowest electronic states, namely $X\,^2\Sigma^+$, $A\,^2\Pi$, $B\,^2\Sigma^+$, $D\,^2\Delta$, $a\,^4\Sigma^+$, $b\,^4\Pi$, were studied using the state-averaged complete active space self consistent field (CASSCF) and multireference configuration interaction (MRCI) methods and aug-cc-pVQZ basis sets. The calculations were performed using C$_{2v}$ point group symmetry. Potential energy curves, illustrated in Fig. 1, spin-orbit coupling and electronic angular moment (Fig. 2), dipole moment curves and transition dipole moment curves (Fig. 3) were computed using MOLPRO2020 (Werner et al. 2020). If the MOLPRO calculations at some geometries did not converge, they were interpolated or extrapolated from the neighbouring points as part of the rovibronic calculations (see below). We used an adaptive *ab initio* grid consisting of 121 bond lengths ranging from 1.1 to 3.08 Å with more points around the equilibrium region of the $X\,^2\Sigma^+$ state centred at 1.585 Å, see Figs. 1–3, where the density of the *ab initio* grid is shown. The grid points with the corresponding *ab initio* values (if converged) are included in the supplementary material.

For *ab initio* calculation we have considered the states of SiN correlating with two dissociation asymptotes, Si(^{3}P) + N(^{4}S) and Si(^{3}P) + N(^{2}D), which generate $^2\Sigma^+$(three states), $^2\Pi$ (one state), $^4\Sigma^+$(one states) and $^4\Pi$ (one state) which show six electronic states, $X\,^2\Sigma^+$, $A\,^2\Pi$, $B\,^2\Sigma^+$, $D\,^2\Delta$, $a\,^4\Sigma^+$ and $b\,^4\Pi$ which are mentioned above in *ab initio* model section. Under the C$_{2v}$ point group symmetry, A_1 corresponds to Σ^+/Δ. Thus, the $^2\Delta$ state arose from the calculation of $^2\Sigma^+$. Molecular orbitals for the subsequent CI calculations were obtained for each spin and symmetry species from state averaged CASSCF calculations (Werner & Knowles 1985; Knowles & Werner 1985) where the state averaging was achieved over all six electronic states considered in this work.

Within the C$_{2v}$ point group symmetry 14 (8σ, $3\pi_x$, $3\pi_y$) orbitals which contained 6 closed (4σ, $1\pi_x$, $1\pi_y$) orbitals were used for all *ab initio* calculations. Thus, the active space represents 8 active (4σ, $2\pi_x$, $2\pi_y$) orbitals with 9 active electrons and spans the valence orbitals 5σ–8σ,2π, 3π. All CI calculations were carried out with the internally contracted CI method (Werner & Knowles 1988; Knowles & Werner 1988). The CI calculations used the same set of reference configurations used in the CASSCF calculation.

The EAMCs represent the L_x and L_y matrix elements, which are important for the accurate description of the lambda doubling effects in Π states originating from the interactions with the Σ and Δ states. In Fig. 2 (right) the L_x components are shown, with L_y related to them by symmetry.
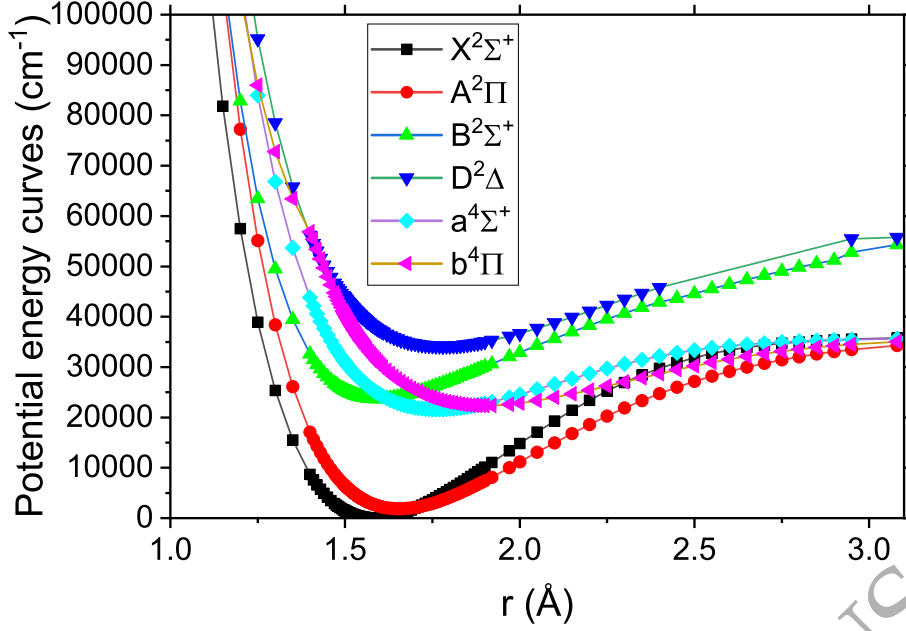
Figure 1. *Ab initio* PECs calculated at the icMRCI level of theory using aug-cc-pVQZ basis set. The grid was specifically made denser around the equilibrium points of the $X\,^2\Sigma^+$ and $A\,^2\Pi$ states.
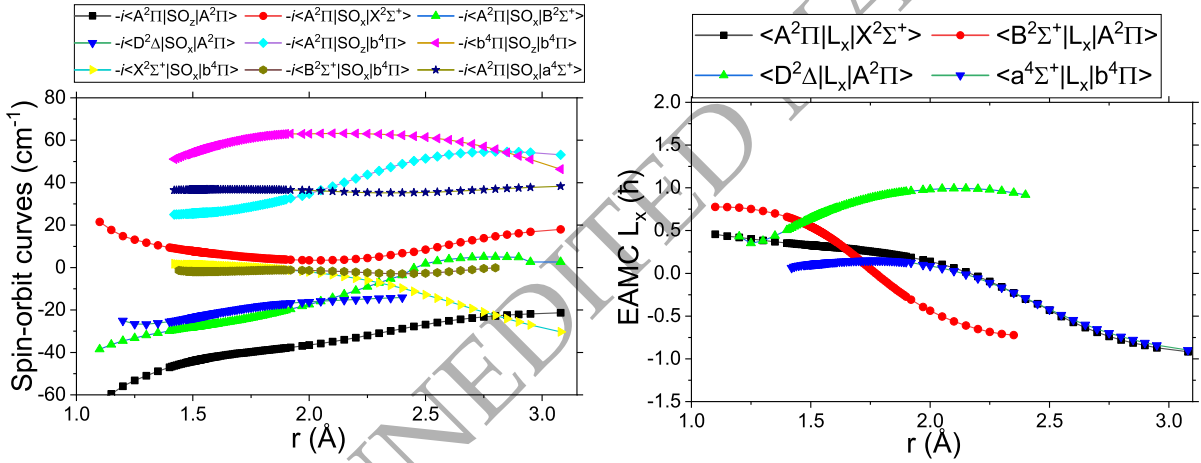

Figure 2. *Ab initio* coupling curves of SiN at the icMRCI/aug-cc-pVQZ level of theory. Left: spin-orbit matrix elements $\langle i|\mathrm{SO}|j\rangle$ for SiN at the icMRCI level of theory using aug-cc-pVQZ basis set. The MOLPRO values of the magnetic quantum numbers M_S (Σ) for the curves can be found in Table 1. Right: Electronic angular momentum L_x curves.

The definition of SOCs, which help form a complete and self-consistent description of a spectroscopic model, requires knowledge of the magnetic quantum numbers M_S (i.e. the projection of the electronic spin Σ), which are specified in Table 1.

All of the *ab initio* curves are later mapped to a different, denser grid used in the solution of the rovibronic problem via interpolation and extrapolation as described in the Spectroscopic Model section below.

The (transition) DMCs $A\,^2\Pi$–$X\,^2\Sigma^+$, $B\,^2\Sigma^+$–$X\,^2\Sigma^+$, $B\,^2\Sigma^+$–$A\,^2\Pi$, $D\,^2\Delta$–$A\,^2\Pi$, $a\,^4\Sigma^+$–$b\,^4\Pi$, and DMCs $X\,^2\Sigma^+$–$X\,^2\Sigma^+$, $A\,^2\Pi$–$A\,^2\Pi$, $B\,^2\Sigma^+$–$B\,^2\Sigma^+$, $D\,^2\Delta$–$D\,^2\Delta$, $a\,^4\Sigma^+$–$a\,^4\Sigma^+$ and $b\,^4\Pi$–$b\,^4\Pi$ were calculated *ab initio* at the same level of theory as the PECs and are shown in Fig. 3. The phases of these non-diagonal TDMCs were selected to be consistent with the phases of the *ab initio* curves produced in our MOLPRO calculations (Patrascu et al. 2014). There is a discontinuity in $\langle X\,^2\Sigma^+|\mu_x|B\,^2\Sigma^+\rangle$ at 2.5 Å that we attribute to the interaction with the higher electronic states, which are not included in this model. Due to the large displacement from the equilibrium corresponding to very high energies this discontinuity does not provide any material effect on our results, as can be seen from the spectra reproduced below.
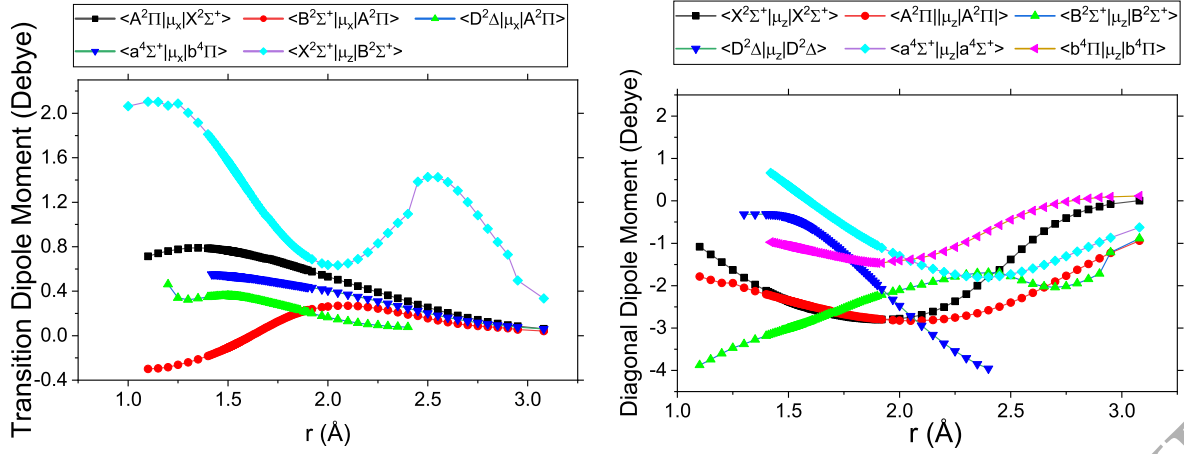
Figure 3. *Ab initio* transitional and diagonal dipole moment curves calculated at the icMRCI level of theory using aug-cc-pVQZ basis set.

Table 1. MOLPRO magnetic quantum numbers M_S values (also known as Σ, projection of $\hat{S}$ along the body fixed z axis) for the *ab initio* spin-orbit matrix elements displayed in Fig. 2.

SOC	bra M_S	ket M_S
$\langle\, A\,^2\Pi_y\ \|SO_x\|X\,^2\Sigma^+\rangle$	-0.5	0.5
$\langle\, A\,^2\Pi_y\ \|SO_x\|B\,^2\Sigma^+\rangle$	-0.5	0.5
$\langle\, A\,^2\Pi_y\ \|SO_x\|a\,^4\Sigma^+\rangle$	-0.5	0.5
$\langle\, D\,^2\Delta_{xy}\ \|SO_x\|A\,^2\Pi_y\rangle$	-0.5	0.5
$\langle\, X\,^2\Sigma^+\|SO_x\|b\,^4\Pi_y\rangle$	0.5	-0.5
$\langle\, B\,^2\Sigma^+\|SO_x\|b\,^4\Pi_y\rangle$	0.5	-0.5
$\langle\, A\,^2\Pi_x\ \|SO_z\|A\,^2\Pi_x\rangle$	0.5	0.5
$\langle\, A\,^2\Pi_x\ \|SO_z\|b\,^4\Pi_x\rangle$	0.5	0.5
$\langle\, b\,^4\Pi_x\ \|SO_z\|b\,^4\Pi_x\rangle$	0.5	0.5

3   MARVEL

All available experimental transition frequencies of SiN were extracted from the published spectroscopic literature and analysed using the MARVEL procedure (Furtenbacher et al. 2007; Császár et al. 2007; Furtenbacher & Császár 2012; Tóbiás et al. 2019). This procedure takes a set of assigned transition frequencies with measurement uncertainties and converts it into a consistent set of empirical energy levels with the uncertainties propagated from the input transitions. The transition data extracted as part of this work from the literature covers the three main bands of SiN involving the $X\,^2\Sigma^+$, $A\,^2\Pi$, and $B\,^2\Sigma^+$ electronic states: $X\,^2\Sigma^+$–$X\,^2\Sigma^+$, $A\,^2\Pi$–$X\,^2\Sigma^+$ and $B\,^2\Sigma^+$–$X\,^2\Sigma^+$, as summarised in Table 2.

3.1   Description of experimental sources

All the available sources of experimental transitions considered in this work are listed below:

92ElHaGu by Elhanine et al. (1992): an infrared (IR) study of the $A\,^2\Pi$–$X\,^2\Sigma^+$ system through 724 transitions. Unfortunately, the original line data with assignments were lost/unavailable and only the derived spectroscopic constants for $A\,^2\Pi$ and $X\,^2\Sigma^+$ states remain. Using their $X\,^2\Sigma^+$ constants we produced four $X\,^2\Sigma^+$–$X\,^2\Sigma^+$ pseudo-experimental lines (MARVEL Magic numbers) to help connecting spectroscopic networks in the MARVEL analysis. We also used their extended set of the spectroscopic constants in PGOPHER (Western 2017) to generate pseudo-experimental energies for the first five vibrational states of $A\,^2\Pi$ and the first three vibrational states of $X\,^2\Sigma^+$ states (up to $J = 49.5$) for the refinement of our spectroscopic model (see below). Elhanine et al. (1992) is the only existing information on the vibrationally excited $A\,^2\Pi$ states of SiN and is therefore crucial for providing MARVEL energies for states of $A\,^2\Pi$ with $v > 1$. The PGOPHER file used to generate the energies for fitting is provided as part of the supplementary information.

85FoLuAm by Foster et al. (1985): This IR observation reported 187 lines of the $A\,^2\Pi$–$X\,^2\Sigma^+$ system originally assigned to the (2,0) band and 6 microwave transitions in the $X\,^2\Sigma^+$–$X\,^2\Sigma^+$ system. This band was later reassigned to 1–0 by Yamada et al. (1988).

85YaHiXX by Yamada & Hirota (1985): This IR study reported 170 lines of the $A\,^2\Pi$–$X\,^2\Sigma^+$ system originally assigned to the (1,0) band, which however was later reassigned to (0,0) by Yamada et al. (1988).

76BrDuHo by Bredohl et al. (1976): This is a UV study of the $B\,^2\Sigma^+$–$X\,^2\Sigma^+$ system. Only spectroscopic constants

Table 2. Breakdown of the assigned transitions by electronic bands for the sources used in this MARVEL study. A and V are the numbers of the available and validated transitions, respectively. The mean and maximum uncertainties (Unc.) obtained using the MARVEL procedure are given in cm^{-1}.

Electronic Band	Vibrational Bands	J Range	A/V	WN range cm^{-1}	Unc. (Mean/Max)
29JeDeXX					
$B\,^2\Sigma^+$–$X\,^2\Sigma^+$	(0,0),(1,1),(2,2),(3,2),(3,3)	0.5–43.5	1060/1355	23267–24279	0.100/0.197
	(4,3),(4,4),(5,4),(5,5),(6,5)	0.5–43.5			
68NaVexx					
$B\,^2\Sigma^+$–$X\,^2\Sigma^+$	(0,0),(1,1),(2,2)	0.5–44.5	420/422.0	23876–24280	0.030/0.191
76BrDuHo					
$B\,^2\Sigma^+$–$X\,^2\Sigma^+$	(1,0),(2,0)	0.5–1.5	4/4	25236–26203	0.100/0.100
84YaHiXX					
$A\,^2\Pi$–$X\,^2\Sigma^+$	(0,0)	0.5–31.5	195/195	1918–2037	0.007/0.007
85FoLuAm $A\,^2\Pi$–$X\,^2\Sigma^+$	(1,0)	0.5–36.5	199/199	2917–3039	0.001/1.00×10^{-3}
$X\,^2\Sigma^+$–$X\,^2\Sigma^+$	(0,0)	0.5–4.5	6/6	2.9039–5.8329	1.00×10^{-3}/1.00×10^{-3}
92ElHaGu $X\,^2\Sigma^+$-$X\,^2\Sigma^+$	(1,0),(2,0)	0.5–1.5	4/4	1140–2267	0.100/0.100

were reported, which we used to generate four pseudo-experimental $B\,^2\Sigma^+$–$X\,^2\Sigma^+$ lines using PGOPHER to help connect the MARVEL inputs into a single spectroscopic network with $J' = 1.5\ B\,^2\Sigma^+ \longleftarrow J" = 0.5\ A\,^2\Pi$ for the (1,0) and (2,0) bands (e and f).

75Linton by Linton (1975): This UV study reported 460 lines of the $C\,^2\Pi$–$A\,^2\Pi$ system. Sadly due to the low quality of this data and the lack of information provided in the paper to reconstruct the full set of quantum numbers required for MARVEL, this source is omitted from the MARVEL analysis of the current work, but the original lines scanned using OCR (optical character reader) software are still provided as part of the supplementary information.

68NaVe by Nagaraj & Verma (1968): This UV study reported 422 lines of the $B\,^2\Sigma^+$–$X\,^2\Sigma^+$ system covering the (0,0), (1,1), (2,2) bands. Originally the spectra was assigned to the SiO$^+$ molecules, but that was reassigned to SiN later as per the correction in Dunn et al. (1969).

29JeDe by Jenkins & de Laszlo (1928): This 1929 work is still the most extensive to date UV observation of the $B\,^2\Sigma^+$–$X\,^2\Sigma^+$ system of SiN reporting 1355 lines from the (0,0), (1,1), (2,2), (3,3), (4,4), (3,2), (4,3), (5,4), (6,5) vibronic bands.

In total, 1987 experimental and 9 pseudo-experimental transitions were processed via the online MARVEL app (available through a user-friendly web interface at http://kkrk.chem.elte.hu/marvelonline) using the Cholesky (analytic) approach with a 0.5 cm^{-1} threshold on the uncertainty of the "very bad" lines. The final MARVEL process for ^{28}Si^{14}N resulted in one main spectroscopic network, containing 1054 energy levels and 1456 validated transitions, with the rotational excitation up to $J = 44.5$ and covering energies up to 30 308 cm^{-1}. These energy levels in conjunction with energies generated from PGOPHER were used to refine our *ab initio* rovibronic spectroscopic model (PECs, SOCs and EAMCs) presented above. The MARVEL input transitions and output energy files are given as part of the supplementary material.

4 ROVIBRONIC CALCULATIONS

To obtain rovibronic energies and wavefunctions for the six electronic states in question, we solve a set of fully coupled Schrödinger equation for the motion of nuclei using the Duo program (Yurchenko et al. 2016). Duo uses the Hunds case a basis set with the vibrational basis functions obtained by solving uncoupled vibrational Schrödinger equations for each electronic state in question with using a sinc DVR basis set (Guardiola & Ros 1982). Atomic masses are used to represent the kinetic energy operator. In Duo calculations, an equidistant grid of 501 radial points ranging from 1.1 to 5.0 Å. The *ab initio* curves were cubic-spline interpolated to map the *ab initio* curves onto the denser Duo grid. For the extension outside the *ab initio* bond lengths ($r > 3.080$ Å), the *ab initio* curves were extrapolated using the functional forms given by (Yurchenko et al. 2016)

$$
\begin{aligned}
f_{\mathrm{PEC}}^{\mathrm{short}}(r) &= A + B/r, \\
f_{\mathrm{TDMC}}^{\mathrm{short}}(r) &= Ar + Br^2, \\
f_{\mathrm{other}}^{\mathrm{short}}(r) &= A + Br,
\end{aligned}
\tag{1}
$$

for short range and

$$
\begin{aligned}
f_{\mathrm{PEC}}^{\mathrm{long}}(r) &= A + B/r^6 \\
f_{\mathrm{EAMC}}^{\mathrm{long}}(r) &= A + Br, \\
f_{\mathrm{other}}^{\mathrm{long}}(r) &= A/r^2 + B/r^3
\end{aligned}
\tag{2}
$$
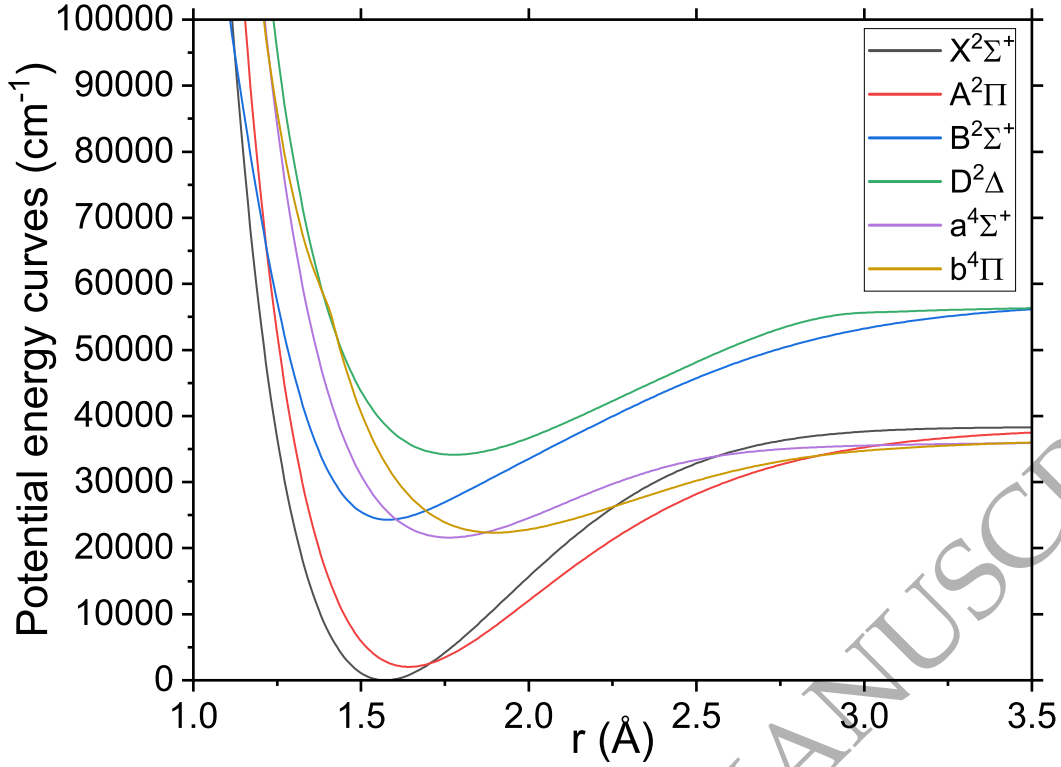
Figure 4. Potential energy curves of SiN representing our final spectroscopic and used in the Duo calculations: $X\,^2\Sigma^+$, $A\,^2\Pi$ and $B\,^2\Sigma^+$ are refined while $D\,^2\Delta$, $a\,^4\Sigma^+$ and $b\,^4\Pi$ are *ab initio*.

for long range, where A and B are stitching parameters. A more detailed description of the Duo methodology was previously given by Yurchenko et al. (2016), see also Tennyson et al. (2016b).

4.1   Refining the spectroscopic model

For our spectroscopic model of SiN we initially used *ab initio* PECs for the doublets $X\,^2\Sigma^+$, $A\,^2\Pi$, $B\,^2\Sigma^+$, $D\,^2\Delta$ and quartets $b\,^4\Pi$, $a\,^4\Sigma^+$, as well as all appropriate SOCs and EAMCs of SiN. The $X\,^2\Sigma^+$, $A\,^2\Pi$ and $B\,^2\Sigma^+$ PECs and the associated couplings were then refined by fitting to our empirical set of MARVEL and PGOPHER term values of ^{28}Si^{14}N as described above.

For the refinements, the PECs for the $X\,^2\Sigma^+$, $A\,^2\Pi$, and $B\,^2\Sigma^+$ states were parameterised using the Extended Morse Oscillator (EMO) function (Lee et al. 1999) as given by

$$V(r) = V_{\mathrm{e}} \;\; + \;\; (A_{\mathrm{e}} - V_{\mathrm{e}}) \left[1 \;\; - \;\; \exp\left(-\sum_{k=0}^{N} B_k \xi_p^k (r - r_{\mathrm{e}}) \right) \right]^2, \tag{3}$$

where $A_{\mathrm{e}} - V_{\mathrm{e}} = D_{\mathrm{e}}$ is the dissociation energy, A_{e} is the corresponding asymptote, r_{e} is an equilibrium distance, and ξ_p is the Šurkus variable (Šurkus et al. 1984) given by

$$\xi_p = \frac{r^p - r_{\mathrm{e}}^p}{r^p + r_{\mathrm{e}}^p} \tag{4}$$

with $V_{\mathrm{e}} = 0$ for the $X\,^2\Sigma^+$ state. The $X\,^2\Sigma^+$ and $A\,^2\Pi$ states have a common asymptote which was fixed for the analytical form of the potential to the ground state dissociation energy D_{e} 4.75 eV based on the experiment by Naulin et al. (1993) (see also Kerkines & Mavridis (2005)). Similarly the $B\,^2\Sigma^+$ state was adjusted to be 19233 cm^{-1} above the $X\,^2\Sigma^+$ dissociation using the atomic excitation energy of N (Kramida et al. 2021). The processed and refined PECs used in Duo can be seen in Fig. 4.

For the parameterisation of SOCs and the EAMCs, the *ab initio* curves were morphed using a polynomial decay expansion
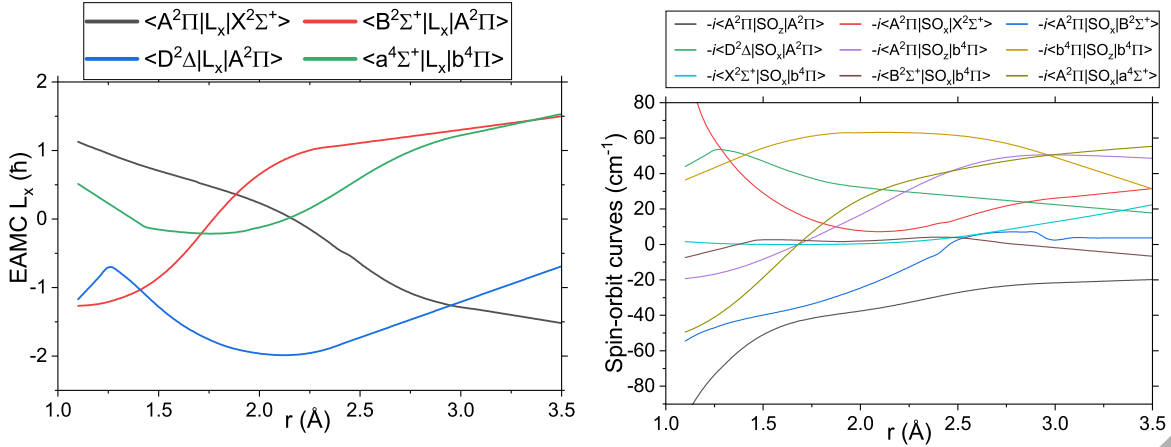
Figure 5. Refined electronic angular momentum and spin-orbit curves for SiN. The MOLPRO values of the magnetic quantum numbers M_S for the SOCs can be found in Table. 1
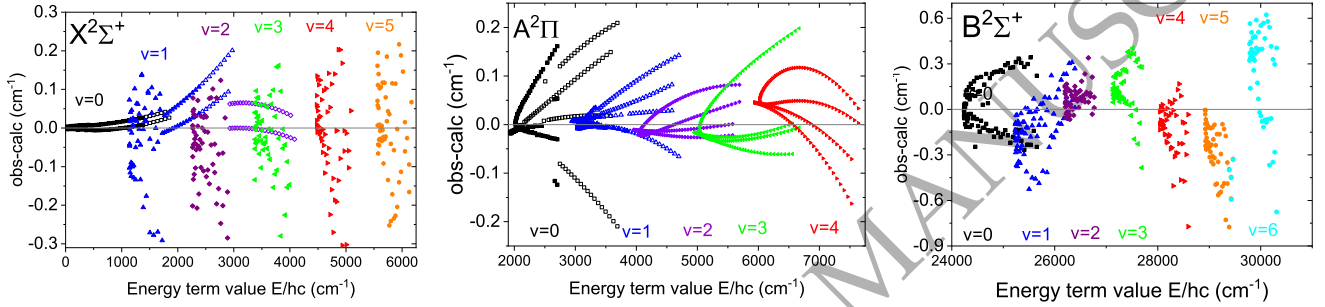
Figure 6. The residuals (Obs.-Calc.) between the experimentally determined energies of SiN ($X\,^2\Sigma^+$, $A\,^2\Pi$ and $B\,^2\Sigma^+$) from our MARVEL analysis (open), pseudo-experimental PGOPHER (filled) generated energies and Duo energies corresponding to our refined spectroscopic model. Only MARVEL energies are available for $B\,^2\Sigma^+$, hence the vibrational level labels are not differentiated by source.

as given by:

$$F(r) = \sum_{k=0}^{N} B_k\, z^k (1 - \xi_p) + \xi_p\, B_\infty, \tag{5}$$

where z is the damped-coordinate polynomial given by:

$$z = (r - r_{\text{ref}})\, e^{-\beta_2 (r - r_{\text{ref}})^2 - \beta_4 (r - r_{\text{ref}})^4}. \tag{6}$$

The refined curves $f(r)$ are the represented as

$$f(r) = F(R) f^{\text{ai}}(r),$$

with $B_\infty = 1$ in order for $F(r) \to 1$ at $r \to \infty$. Morphing allows one to retain the original shape of the property with a minimum number of varied parameters, see e.g. Prajapat et al. (2017) and Yurchenko et al. (2018). In Eq. (6), r_{ref} is a reference position chosen to be close to r_e of $X\,^2\Sigma^+$ and β_2 and β_4 are damping factors, typically chosen to be 8×10^{-1} and 2×10^{-2}. The morphed and extended by Duo SOCs and EAMCs are shown in Fig. 5.

The 1062 MARVEL and 854 PGOPHER energy levels values were used to refine the PECs, SOCs, EAMCs into analytical form as described above. Figure 6 shows the residuals representing how well our model compares to the MARVEL and PGOPHER energies. Unfortunately the most significant work from the number of transitions provided is Jenkins & de Laszlo (1928), where the accuracy of the transitions was 0.1 cm^{-1} at best. This is the main reason for the spread of uncertainties in the $X\,^2\Sigma^+$ and $B\,^2\Sigma^+$ states. Similarly most data for the $A\,^2\Pi$ state had to be supplemented using the PGOPHER calculations due to the difficulty of obtaining experimental data for the state.

4.2 Dipole moment curves

Most of the (transition) dipole moment curves from Fig. 3 were left unchanged and used as grid points in Duo calculations apart from the $\langle X\,^2\Sigma^+ | \mu_z | X\,^2\Sigma^+ \rangle$, which was fitted to analytical form of the polynomial decay given in Eq. (5). Having an
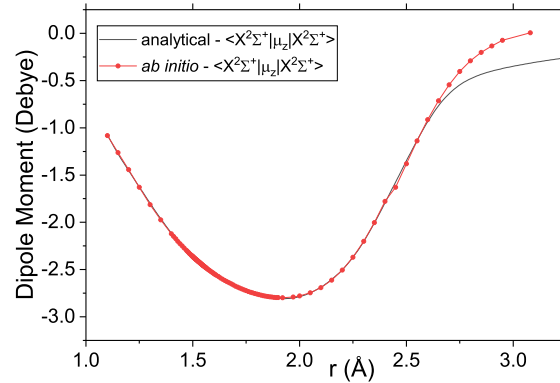
Figure 7. Comparison of the *ab initio* and fitted DMC for the $X\,^2\Sigma^+$–$X\,^2\Sigma^+$ system.

Table 3. Line list statistics for each isotopologue of SiN.

Isotopologue	g_{ns}	N_{states}	N_{trans}
^{28}Si^{14}N	3	131935	43646806
^{29}Si^{14}N	6	132335	43946969
^{30}Si^{14}N	3	132706	44223730
^{28}Si^{15}N	2	133460	44816182

g_{ns}: Nuclear spin degeneracy;
N_{states}: Number of states;
N_{trans}: Number of transitions.

analytical form helps to reduce the numerical noise arising due to interpolation of *ab initio* curves present in high overtone transitions, see Medvedev et al. (2016). The comparison between *ab initio* $X\,^2\Sigma^+$–$X\,^2\Sigma^+$ DMC and its analytical form is shown in Fig. 7, with the deviations at very large radial displacement not affecting the intensities for the energy excitations selected for this study.

All expansion parameters or curves defining our spectroscopic model are given as supplementary material to the paper as a Duo input file.

5   LINE LIST AND SIMULATIONS OF SPECTRA OF SIN

The SiNful line list was produced with Duo using the empirically refined and *ab initio* curves as described above. For the main isotopologue ^{28}Si^{14}N, it contains 43 646 806 transitions and 131 935 states for $X\,^2\Sigma^+$, $A\,^2\Pi$, $B\,^2\Sigma^+$, $D\,^2\Delta$, $a\,^4\Sigma^+$ and $b\,^4\Pi$, covering wavenumbers up to 58 000 cm^{-1} $v = 0\ldots30$ and $J = 0\ldots245.5$. For the isotopologue line lists only the atomic masses were adjusted in the Duo input files. Further details on the line list statistics covering the isotpologues can be seen in Table 3. The line list is provided in State and Transition files, as is customary for the ExoMol format (Tennyson et al. 2020). Extracts from the States and Trans files are shown in Tables 4 and 5, respectively; the full files are available from www.exomol.com. The States file contains energy term values, state uncertainties, Landé-g factors (Semenov et al. 2017), lifetimes (Tennyson et al. 2016a) and quantum numbers. The Transition file contains Einstein A coefficients. The partition functions are also included as part the standard line list compilation.

The calculated energies were replaced with the MARVEL values (MARVELised), where available. We have used the labels 'Ca','EH' and 'Ma' in the penultimate column of the States file to indicate if the energy value is calculated using Duo, derived using PGOPHER or MARVELised, respectively.

The uncertainty values in the States file correspond to two cases: the MARVEL uncertainties are used for MARVELised energies, while for the calculated values the following approximate expression is used:

$$\text{unc} = av + bJ(J+1), \tag{7}$$

where a and b are electronic state dependent constant, given in Table 6. For the $X\,^2\Sigma^+$, $A\,^2\Pi$ and $B\,^2\Sigma^+$ states uncertainties were estimated based on the progression of residuals from Fig. 6 as average increases of obs.-calc. in v and J for each state shown.

Table 4. An extract from the states file of the SiNful line list for ^{28}Si^{14}N.

i	Energy (cm^{-1})	g_i	J	unc	τ	g	Parity		State	v	Λ	Σ	Ω	Label	Calc.
2	1138.471940	6	0.5	0.200000	0.5211	2.001919	+	e	X2Sigma+	1	0	0.5	0.5	Ma	1138.405398
3	2017.654928	6	0.5	0.010000	0.0015	0.000607	+	e	A2Pi	0	1	-0.5	0.5	Ma	2017.651598
4	2263.632470	6	0.5	0.400000	0.1714	2.000967	+	e	X2Sigma+	2	0	0.5	0.5	Ma	2263.834585
5	3037.121068	6	0.5	0.006000	0.0006	0.000570	+	e	A2Pi	1	1	-0.5	0.5	Ma	3037.120364
6	3375.983139	6	0.5	1.000000	0.0368	2.001071	+	e	X2Sigma+	3	0	0.5	0.5	Ma	3376.117442
7	4044.188981	6	0.5	0.200375	0.0004	0.000245	+	e	A2Pi	2	1	-0.5	0.5	EH	4044.208257
8	4475.345990	6	0.5	1.600000	0.0124	2.001414	+	e	X2Sigma+	4	0	0.5	0.5	Ma	4475.285785
9	5038.850133	6	0.5	0.300375	0.0003	-0.000102	+	e	A2Pi	3	1	-0.5	0.5	EH	5038.860507
10	5561.363517	6	0.5	0.100750	0.0057	2.001737	+	e	X2Sigma+	5	0	0.5	0.5	Ca	5561.363517
11	6021.067289	6	0.5	0.400375	0.0002	-0.000370	+	e	A2Pi	4	1	-0.5	0.5	EH	6021.017509
12	6634.354317	6	0.5	0.120750	0.0032	2.001917	+	e	X2Sigma+	6	0	0.5	0.5	Ca	6634.354317
13	6990.593938	6	0.5	0.500375	0.0002	-0.000488	+	e	A2Pi	5	1	-0.5	0.5	Ca	6990.593938
14	7694.239922	6	0.5	0.140750	0.0020	2.001777	+	e	X2Sigma+	7	0	0.5	0.5	Ca	7694.239922
15	7947.534233	6	0.5	0.600375	0.0002	-0.000299	+	e	A2Pi	6	1	-0.5	0.5	Ca	7947.534233
16	8740.963173	6	0.5	0.160750	0.0014	2.000443	+	e	X2Sigma+	8	0	0.5	0.5	Ca	8740.963173
17	8891.787413	6	0.5	0.700375	0.0001	0.001068	+	e	A2Pi	7	1	-0.5	0.5	Ca	8891.787413

i: State counting number.
$\tilde{E}$: State energy term values in cm^{-1}.
g_i: Total statistical weight, equal to $g_{\mathrm{ns}}(2J+1)$.
J: Total angular momentum.
unc: Uncertainty, cm^{-1}.
τ: Lifetime (s^{-1}).
g: Landé g-factors.
$+/-$: Total parity.
State: Electronic state.
v: State vibrational quantum number.
Λ: Projection of the electronic angular momentum.
Σ: Projection of the electronic spin.
Ω: Projection of the total angular momentum, $\Omega = \Lambda + \Sigma$.
Label: 'Ma' is for MARVEL,'EH' is PGOPHER generated and 'Ca' is for Calculated (using Duo).

Table 5. An extract from the transitions file of the SiNful line list for ^{28}Si^{14}N.

f	i	A_{fi} (s^{-1})	$\tilde{\nu}_{fi}$
34822	33867	6.3723E+01	4047.041414
2808	2455	2.0314E-04	4047.041433
63044	62682	1.4457E-06	4047.041573
61850	60890	1.5342E-01	4047.042750
65187	65424	1.1950E+02	4047.042900
75707	75959	2.7837E+00	4047.043952
37830	36872	9.1146E-02	4047.044029
49826	49468	9.3588E-04	4047.044408
18065	18306	6.1554E+01	4047.045440
53117	53365	5.3547E-02	4047.046876
70272	69910	5.1581E-03	4047.047010
106232	106467	5.6296E-01	4047.047815

f: Upper state counting number;
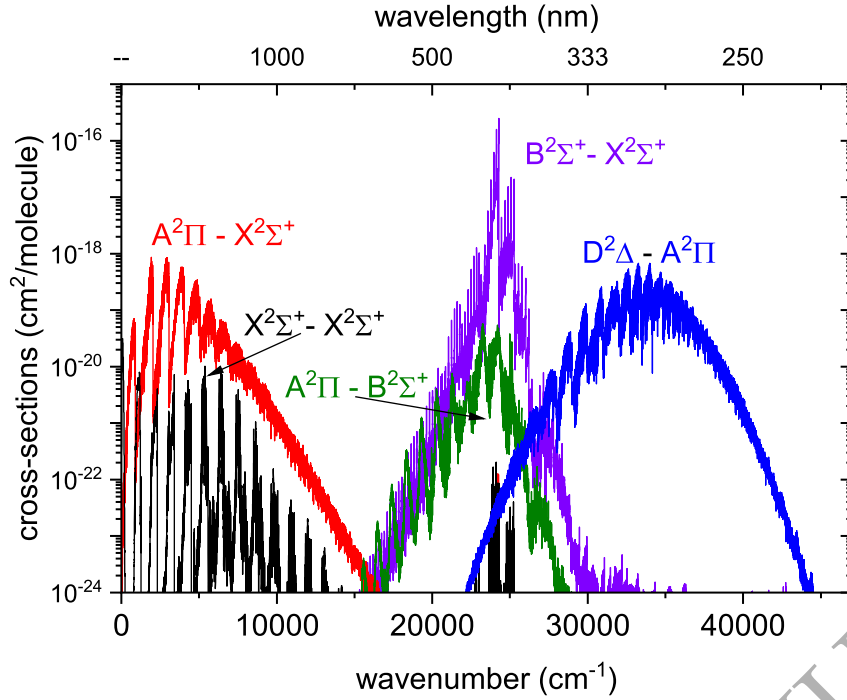i: Lower state counting number;
A_{fi}: Einstein-A coefficient in s^{-1};
$\tilde{\nu}_{fi}$: transition wavenumber in cm^{-1}.

Table 6. a and b constants (cm^{-1}) defining state dependent uncertainties via Eq. (7).

State	a	b
$X\,^2\Sigma^+$	0.02	0.001
$A\,^2\Pi$	0.1	0.001
$B\,^2\Sigma^+$	0.5	0.001
All other	0.8	0.001

Figure 8. Simulated absorption spectrum of SiN at 2000 K showing the main bands of the system. A Gaussian profile of the half width of half maximum (HWHM) of 1 cm^{-1} was used.

5.1 Overall Spectra

To demonstrate the accuracy of the SiNful line list, several spectra were calculated, analysed and compared to available laboratory measurements. Figure 8 illustrates the main bands of SiN at 2000 K. The dominance of the $X\,^2\Sigma^+$–$A\,^2\Pi$ in the 0–5000 cm^{-1} region confirms why it is hard to detect the comparatively weak $X\,^2\Sigma^+$–$X\,^2\Sigma^+$ transitions. Additionally, while the $X\,^2\Sigma^+$–$B\,^2\Sigma^+$ band system appears to be overall stronger than $A\,^2\Pi$– $B\,^2\Sigma^+$, the latter should still be detectable in the 18000 – 24000 cm^{-1} region according to our model, in line with observations of these vibronic bands by Ojha & Gopal (2006) and Foster et al. (1985). Additionally, in the region above 28000 cm^{-1} the $A\,^2\Pi$ -$D\,^2\Delta$ band becomes dominant, which agrees with previous vibronic observations in this region by Bredohl et al. (1976). Figure 9 shows how the spectrum of ^{28}Si^{14}N changes with increasing temperature.

5.2 $B\,^2\Sigma^+$–$X\,^2\Sigma^+$ band

$B\,^2\Sigma^+$–$X\,^2\Sigma^+$ is the strongest electronic band in the system, with the largest number of experimental observations due to it being the easiest to detect. In Figure 10 we simulate the $B\,^2\Sigma^+$–$X\,^2\Sigma^+$ (5,4) and (4,3) band at rotational temperature of 392 K and 412 K respectively to provide direct comparison with the experiment. The simulated spectra is also adjusted to be in air rather than in vacuum to align with the experimental spectra. This is achieved by using the IAU standard of conversion adopted by Morton (1991):

$$\lambda_{\text{air}} = \frac{\lambda_{\text{vacuum}}}{\left(1.0 + 2.735182 \times 10^{-4} + \frac{131.4182}{\lambda_{\text{vac}}^2} + \frac{2.76249 \times 8}{\lambda_{\text{vac}}^4}\right)} \tag{8}$$

where λ_{air} and λ_{vac} are wavelengths in air and vacuum respectively. The overall agreement on the rotational structure is within the uncertainty provided.

5.3 $A\,^2\Pi$–$X\,^2\Sigma^+$ band

The $A\,^2\Pi$–$X\,^2\Sigma^+$ band system was first detected by Jevons (1913), however because of the vicinity of the $A\,^2\Pi$ and $X\,^2\Sigma^+$ states it has proved difficult to study experimentally. Figure 11 shows the comparison of our simulated spectra of the $A\,^2\Pi$– $X\,^2\Sigma^+$ (1,0) band with the experiment of Foster et al. (1985). The spectrum is simulated at the effective temperature of 740 K. The position of the bands agrees to 0.05 cm^{-1} which is within our calculated uncertainties.

Figure 12 shows a comparison of the simulated spectra (shown as sticks) for different silicon isotopes of the SiN molecule
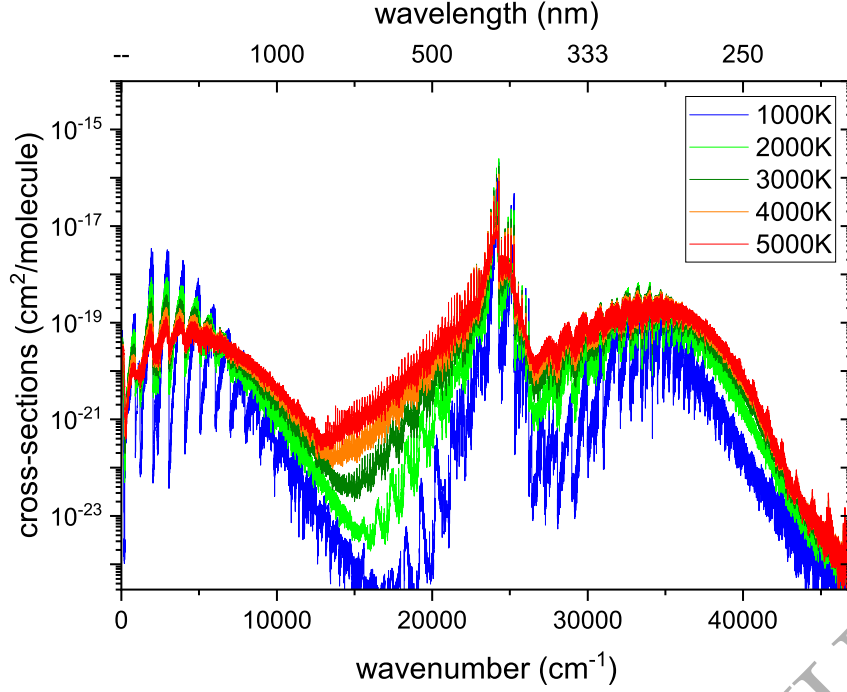
Figure 9. Temperature dependence of the SiN spectra using the SiNful line list. A Gaussian profile with HWHM of 1 cm^{-1} was used.
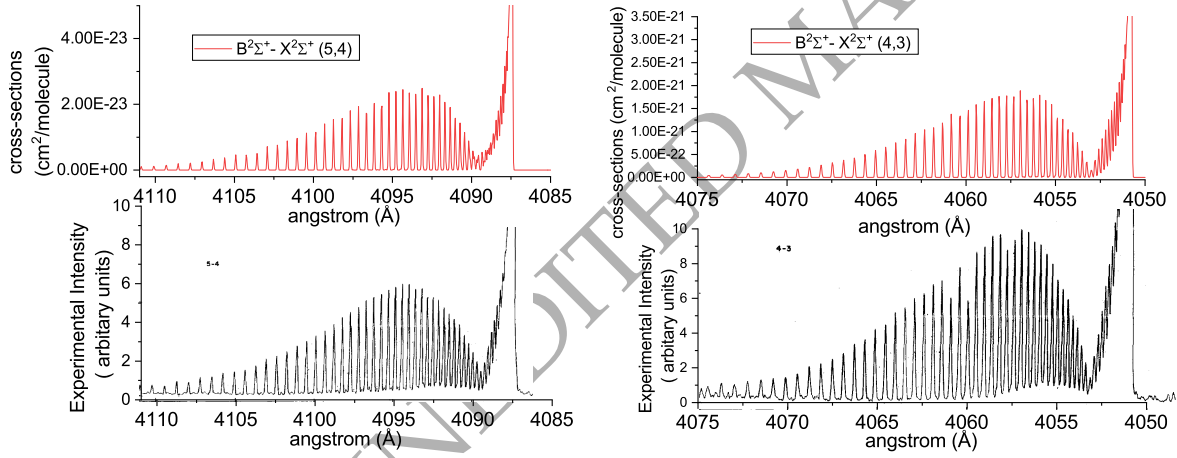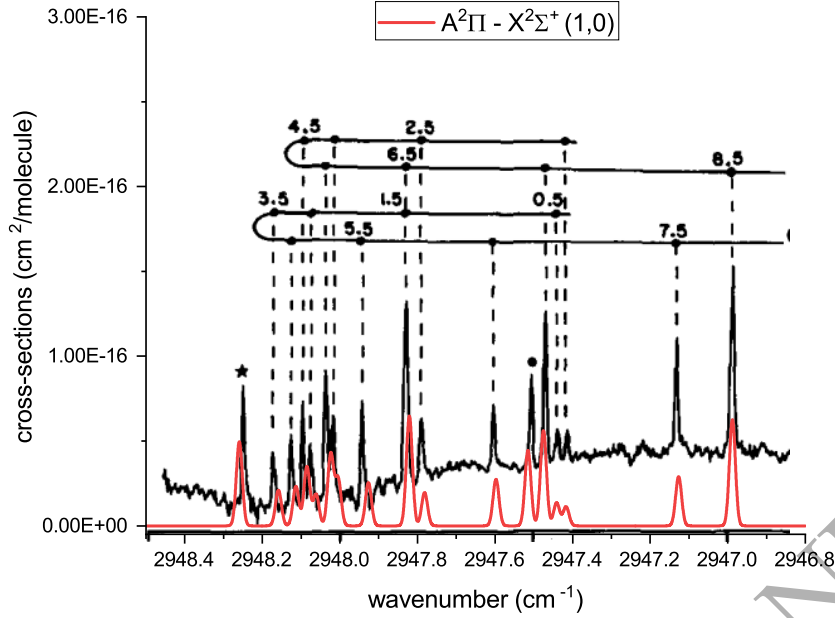

Figure 10. Simulated absorption spectra of SiN showing the $B\,^2\Sigma^+$–$X\,^2\Sigma^+$ (5,4) and (4,3) bands at temperature of 392 K and 412 K respectively. A comparison to the experimental spectra from Schofield & Broida (1965) is provided. A Gaussian profile HWHM of 0.2 cm^{-1} was used.

with the experimental spectra of Yamada et al. (1988). The overall agreement for ^{28}Si^{14}Nis $\sim$0.016 cm^{-1}, for ^{29}Si^{14}N is $\sim$0.035 cm^{-1} and for ^{30}Si^{14}N is $\sim$0.055 cm^{-1}. The intensities were adjusted based on the natural abundance for each silicon isotope. These are defined as 92.2%, 4.68% and 3.09% for ^{28}Si^{14}N ,^{29}Si^{14}N, ^{30}Si^{14}N respectively. Additionally, in the same range a Q$_{22}$(0.5) line of $A\,^2\Pi$–$X\,^2\Sigma^+$ (0,0) for ^{29}Si^{14}N should be present, but it was probably too weak to be observed during the experiment. This line is indicated with the an asterisk.

5.4 Lifetimes

There are few precise experimental measurements of the lifetimes of different electronic states of SiN in the literature. Walkup et al. (1984) report the $B\,^2\Sigma^+$ $v = 1$ vibrational state to have a lifetime of 200 ns $\pm$10 ns ($T_{\rm rot} = 500$ K). Our calculated value for this vibronic state is lower: 130 ns ($J = 0.5$), slowly increasing to 150 ns for $J = 100$ ns and even 200 ns for $J = 160.5$ ($v = 1$, $B\,^2\Sigma^+$). Additionally there have been several theoretical works (Xing et al. 2018; Kaur & Baluja 2015) which showed that for the $A\,^2\Pi$ state the lifetimes decrease with the vibrational levels as lower levels are much less energetically accessible

Figure 11. Simulated absorption spectrum of SiN at effective temperature of 740 K showing the $A\,^2\Pi$–$X\,^2\Sigma^+$ (1,0) band. A Gaussian profile of HWHM of 0.009 cm^{-1} was used. A comparison with the experimental spectra from Foster et al. (1985) is provided, with calculated spectra in red and experimental in black.

Table 7. Comparison of lifetimes from our current work (A) and Xing et al. (2018) (B). An experimental lifetime 200 ± 10 ns was reported by Walkup et al. (1984) for $v' = 1$ of $B\,^2\Sigma^+$.

	$A\,^2\Pi$/ μs		$B\,^2\Sigma^+$/ ns	
v'	A	B	A	B
0	1460	1660	124	129
1	610	679	130	136
2	385	429	137	143
3	281	312	143	150
4	221	245	150	157
5	182	202	156	164
6	155	172	163	170
7	135	149	169	176
8	121	132	175	181
9	109	119	181	187
10	98.3	109	186	192
11	90.5	99.8	192	196
12	84.0	92.6	197	201
13	78.5	86.6	202	205
14	73.9	81.5	207	210

due to the proximity of the $X\,^2\Sigma^+$ state. This can be seen in more detail in Table 7, where we compare our calculated lifetimes with those of Xing et al. (2018); the agreement is good.

5.5 Partition function

For the partition function of ^{28}Si^{14}N, we follow the ExoMol and HITRAN (Gamache et al. 2017) convention and include the full nuclear spin. This means that our convention is different to that of recently reported by Barklem & Collet (2016) with whom we compare our results in Fig. 13. In order for comparison to be in equivalent convention, their partition function
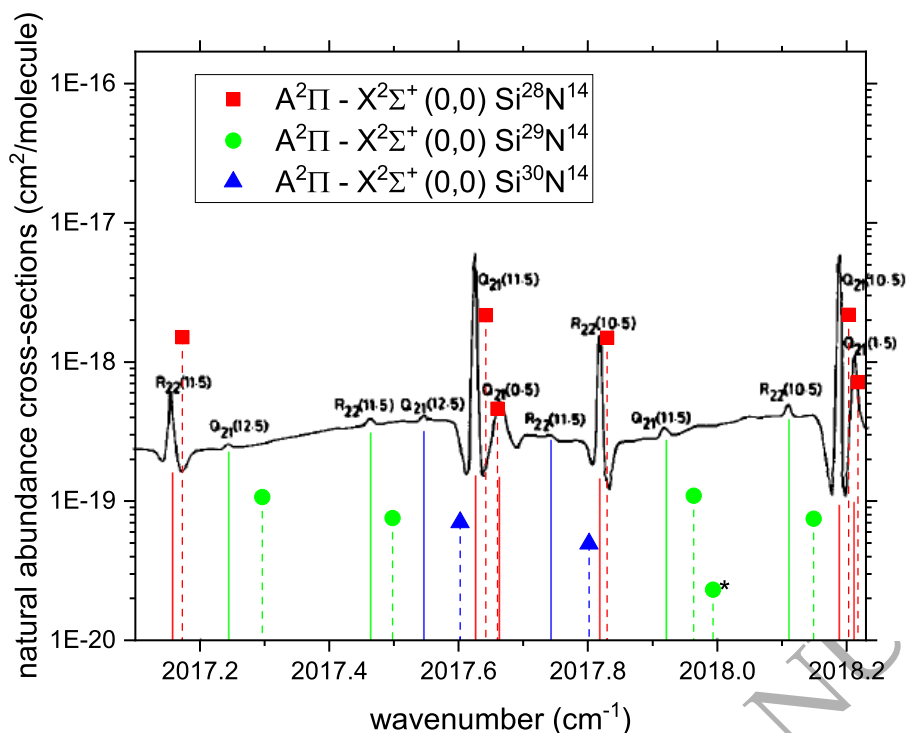
Figure 12. Comparison of the simulated stick spectrum and experimental emission spectrum of the SiN isotpologues (^{28}Si^{14}N, ^{29}Si^{14}N, ^{30}Si^{14}N) at 300 K. Straight lines are experimentally observed line positions and dashed lines with points represent calculated. The asterisk indicates the $Q_{22}(0.5)$ line for ^{29}Si^{14}N not observed experimentally by (Yamada et al. 1988).

was multiplied by the factor of three as ^{14}N has a nuclear spin degeneracy of 3 and ^{28}S has nuclear spin degeneracy of 0. The differences at higher temperatures can be attributed to incompleteness of the model used by Barklem & Collet (2016), which is demonstrated by comparing partition functions by using only $X\,^2\Sigma^+$ state, $X\,^2\Sigma^+$ and $A\,^2\Pi$ states and all states: the partition function of Barklem & Collet (2016) appears to be based on the $X\,^2\Sigma^+$ state only. As evident from Fig. 13, the contribution from the $A\,^2\Pi$ state cannot be neglected due to its low excitation energy.

Partition functions in for $T = 1 - 3000$ K in steps of 1 K are available the 4 isotopologue, ^{28}Si^{14}N, ^{29}Si^{14}N, ^{30}Si^{14}N and ^{28}Si^{15}N, are available via the ExoMol website.

6 CONCLUSION

New IR and UV line lists called SiNful for isotopologues of SiN are presented. SiNful is available from `www.exomol.com` (Tennyson et al. 2020) and from `www.zenodo.org` (European Organization For Nuclear Research & OpenAIRE 2013). As part of the line list construction, a MARVEL analysis for ^{28}Si^{14}N was performed. All experimental line positions from the literature (to the best of our knowledge) currently available for the X–X, A–X and B–X systems were processed to generate a MARVEL set of empirical energies of SiN. An accurate spectroscopic model for SiN was built: *ab initio* (T)DMC and empirically refined PECs, SOCs, EAMCs, using both previously derived MARVEL energies as well as PGOPHER generated energies.

The line list was MARVELised, where the theoretical energies are replaced with the MARVEL values (where available). The line list provides uncertainties of the rovibronic states in order to help in high-resolution applications. Comparisons of simulated spectra with experiment for both A–X and B–X system show close agreement. Additionally lifetimes, Landé-g factors and partition functions are provided. The importance of inclusion of the energies of the excited state $A\,^2\Pi$ when computing the partition function of SiN is demonstrated.
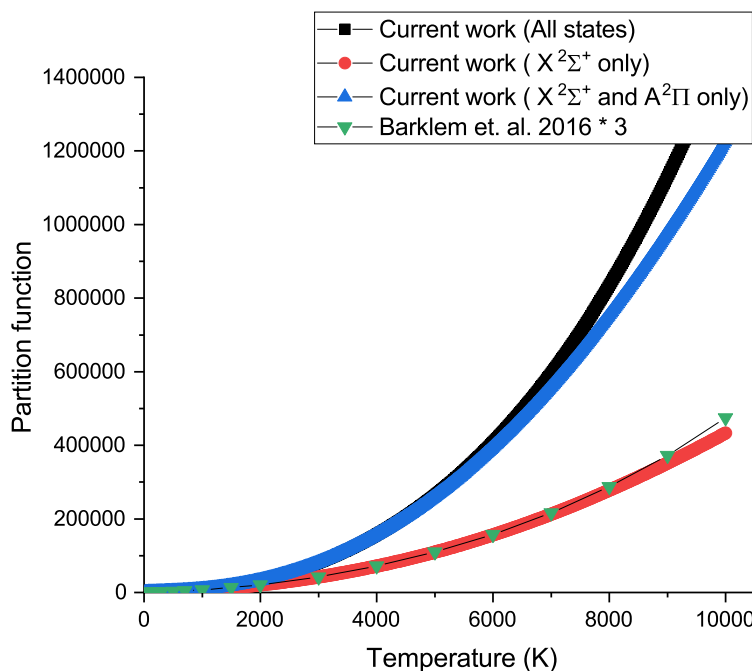
Figure 13. Comparison of the partition functions for ^{28}Si^{14}N: values from this work and the work of Barklem & Collet (2016).

7   DATA AVAILABILITY

The data underlying this article are available in the article and in its online supplementary material, including (1) the Duo input files for each isotopologue containing all the potential energy, (transition) dipole moment and coupling curves of SiN used in this work, (2) the MARVEL data set, (3) digitalised line data from Linton (1975), (4) extracted ab initio curves as part of the excel, (5) PGOPHER file used to generate energy levels for two low lying states, (6) the temperature-dependent partition function of ^{28}Si^{14}N up to 10000 K. The SiNful line lists for ^{28}Si^{14}N, ^{29}Si^{14}N, ^{30}Si^{14}N and ^{28}Si^{15}N are available from www.exomol.com.

REFERENCES

Barklem P. S., Collet R., 2016, A&A, 588, A96
Borin A., 1996, Chem. Phys. Lett., 262, 80
Bredohl H., Dubois I., Houbrechts Y., Singh M., 1976, Can. J. Phys., 54, 680
Brugamyer E., Dodson-Robinson S. E., Cochran W. D., Sneden C., 2011, The Astrophysical Journal, 738, 97
Bruna P., Dohmann H., Peyerimhoff S., 1984, Can. J. Phys., 62, 1508
CRC Handbook 2016, CRC Handbook of Chemistry and Physics, 88th Edition, 97 edn. CRC Press
Cai Z., Martin J., Francois J., 1998, J. Mol. Spectrosc., 188, 27
Chen H., Krasowki M., Fitzgerald G., 1993, J. Chem. Phys., 98, 8710
Chong D., 1994, Chem. Phys. Lett., 220, 102
Császár A. G., Czakó G., Furtenbacher T., Mátyus E., 2007, Annu. Rep. Comput. Chem., 3, 155
Curtiss L. A., Raghavachari K., Trucks G. W., Pople J. A., 1991, J. Chem. Phys., 94, 7221
Davis D., 1947, AJ., 106, 28
Dunn T. M., Rao K. M., Nagaraj S., Verma R. D., 1969, Can. J. Phys., 47, 2128
Elhanine M., Hanoune B., Guelachvili G., Amiot C., 1992, Journal De Physique II, 2, 931
European Organization For Nuclear Research OpenAIRE 2013, Zenodo, doi:10.25495/7GXK-RD71, https://www.zenodo.org/
Feldman P., Matthews H., Bell M., Herzberg G., Saito S., Endo Y., Hirota E., 1983, Journal of the Royal Astronomical Society of Canada, 77, 258

Foster S., 1984, J. Mol. Spectrosc., 106, 369

Foster S., 1989, J. Mol. Spectrosc., 137, 430

Foster S., Lubic K., Amano T., 1985, J. Chem. Phys., 82, 709

Furtenbacher T., Császár A. G., 2012, J. Mol. Struct., 1009, 123

Furtenbacher T., Császár A. G., Tennyson J., 2007, J. Mol. Spectrosc., 245, 115

Gamache R. R., et al., 2017, J. Quant. Spectrosc. Radiat. Transf., 203, 70

Gohel V., Shah N., 1975, Indian Journal of Pure & Applied Physics, 13, 162

Gratton L., 1952, AJ., 115, 346

Guardiola R., Ros J., 1982, J. Chem. Phys., 45, 374

Ito H., Suzuki K., Kondow T., Kuchitsu K., 1993, Chem. Phys. Lett., 208, 328

Jenkins F., de Laszlo H., 1928, Proc. R. Soc. London, Ser. A, 122, 103

Jevons W., 1913, Proc. R. Soc. London, Ser. A, 89, 187

Jungnickel G., Frauenheim T., Jackson K., 2000, J. Chem. Phys., 112, 1295

Kaur S., Baluja K. L., 2015, Eur. Phys. J. D, 69, 89

Kerkines I., Mavridis A., 2005, J. Chem. Phys., 123, 124301

Knowles P. J., Werner H.-J., 1985, Chem. Phys. Lett., 115, 259

Knowles P. J., Werner H.-J., 1988, Chem. Phys. Lett., 145, 514

Kramida A., Ralchenko Y., Reader J., NIST ASD Team 2021, NIST Atomic Spectra Database (ver. 5.9), [Online]. Available: http://physics.nist.gov/asd [2021, October 31]. National Institute of Standards and Technology, Gaithersburg, MD., doi:10.18434/T4W30F

Le Roy R. J., 1998, J. Mol. Spectrosc., 191, 223

Lee E. G., Seto J. Y., Hirao T., Bernath P. F., Le Roy R. J., 1999, J. Mol. Spectrosc., 194, 197

Lee D.-s., Song H.-W., Choi C.-G., Jung M. Y., 2014, Journal of Biomedical Optics, 19, 1

Li B.-X., Wang G.-y., Ding W.-f., Ren X.-j., Ye J.-z., 2009, Physica B: Condensed Matter, 404, 1679

Linton C., 1975, J. Mol. Spectrosc., 55, 108

McDonough W., Sun S.-s., 1995, Chemical Geology, 120, 223

Mclean A., Liu B., Chandler G., 1992, J. Chem. Phys., 97, 8459

Medvedev E. S., Meshkov V. V., Stolyarov A. V., Ushakov V. G., Gordon I. E., 2016, J. Mol. Spectrosc., 330, 36

Melius C., Ho P., 1991, J. Phys. Chem., 95, 1410

Meloni G., Sheehan S., Ferguson M., Neumark D., 2004, J. Phys. Chem. A, 108, 9750

Morton D. C., 1991, ApJS, 77, 119

Muller-Plathe F., Laaksonen L., 1989, Chem. Phys. Lett., 160, 175

Mulliken R., 1925, Phys. Rev., 26, 0319

Nagaraj S., Verma R. D., 1968, Can. J. Phys., 46, 1597

Naulin C., Costes M., Moudden Z., Ghanem N., Dorthe G., 1993, Chem. Phys. Lett., 202, 452

Ojha K. S., Gopal R., 2006, Indian J. Phys., 80, 819

Ojha K. S., Gopal R., 2013, Spectra Chimica Acta A, 109, 155

Oyedepo G. A., Peterson C., Wilson A. K., 2011, J. Chem. Phys., 135, 094103

Oyeyemi V. B., Krisiloff D. B., Keith J. A., Libisch F., Pavone M., Carter E. A., 2014, The Journal of Chemical Physics, 140, 044317

Patrascu A. T., Hill C., Tennyson J., Yurchenko S. N., 2014, J. Chem. Phys., 141, 144312

Pettersson M., Tkachenko S., Schmidt S., Berlind T., Jacobson S., Hultman L., Engqvist H., Persson C., 2013, Journal of the Mechanical Behavior of Biomedical Materials, 25, 41

Piper L. G., Caledonia G. E., 1991, J. Chem. Phys., 95, 698

Prajapat L., Jagoda P., Lodi L., Gorman M. N., Yurchenko S. N., Tennyson J., 2017, MNRAS, 472, 3648

Preuss R., Buenker R., Peyerimhoff S., 1978, J. Mol. Spectrosc., 49, 171

Raza S. M., Khurshid Z., Zafar M. S., Najeeb S., Ul Yaqin S. A., 2020, in Zafar M. S., Khurshid Z., Khan A. S., Najeeb S., Sefat F., eds, Woodhead Publishing Series in Biomaterials, Dental Implants. Woodhead Publishing, pp 287–299, doi:10.1016/B978-0-12-819586-4.00015-9

Schilke P., Leurini S., Menten K., Alcolea J., 2003, A&A, 412, L15

Schofield K., Broida H. P., 1965, Photochemistry and Photobiology, 4, 989

Semenov M., Yurchenko S. N., Tennyson J., 2017, J. Mol. Spectrosc., 330, 57

Serra E., et al., 2018, Journal of Microelectromechanical Systems, 27, 1193

Singh M., Bredohl H., Remy F., Dubois I., 1973, J. Phys. B: At. Mol. Opt. Phys., 6, 2656

Singh P., Sanzovo G., Borin A., Ornellas F., 1999, MNRAS, 303, 235

Stevens A., Ferguson H., 1963, Can. J. Phys., 41, 240

Šurkus A. A., Rakauskas R. J., Bolotin A. B., 1984, Chem. Phys. Lett., 105, 291

Tennyson J., Hulme K., Naim O. K., Yurchenko S. N., 2016a, J. Phys. B: At. Mol. Opt. Phys., 49, 044002

Tennyson J., Lodi L., McKemmish L. K., Yurchenko S. N., 2016b, J. Phys. B: At. Mol. Opt. Phys., 49, 102001

Tennyson J., et al., 2020, J. Quant. Spectrosc. Radiat. Transf., 255, 107228

Tóbiás R., Furtenbacher T., Tennyson J., Császár A. G., 2019, Phys. Chem. Chem. Phys., 21, 3473

Turner B. E., 1992, ApJ, 388, L35

Turner J., Dalgarno A., 1977, ApJ, 213, 386

Vlassiouk I., Apel P. Y., Dmitriev S. N., Healy K., Siwy Z. S., 2009, Proceedings of the National Academy of Sciences, 106, 21039

Walkup R., Avouris P., Dreyfus R. W., Jasinski J. M., Selwyn G. S., 1984, Applied Physics Letters, 45, 372

Werner H.-J., Knowles P. J., 1985, J. Chem. Phys., 82, 5053

Werner H.-J., Knowles P. J., 1988, J. Chem. Phys., 89, 5803

Werner H.-J., et al., 2020, J. Chem. Phys., 152, 144107

Western C. M., 2017, J. Quant. Spectrosc. Radiat. Transf., 186, 221

Xie W., et al., 2017, Advanced Materials, 29, 1604866
Xing W., Shi D., Sun J., Zhu Z., 2013, Eur. Phys. J. D, 67, 228
Xing W., Shi D., Sun J., Zhu Z., 2018, ApJS, 237, 16
Yamada C., Hirota E., 1985, J. Chem. Phys., 82, 2547
Yamada C., Hirota E., Yamamoto S., Saito S., 1988, J. Chem. Phys., 88, 46
Yurchenko S. N., Lodi L., Tennyson J., Stolyarov A. V., 2016, Comput. Phys. Commun., 202, 262
Yurchenko S. N., Sinden F., Lodi L., Hill C., Gorman M. N., Tennyson J., 2018, MNRAS, 473, 5324
Ziurys L., Clemens D., Saykally R., Colvin M., Schaefer H., 1984, AJ., 281, 219